Knifefish turning control and hydrodynamics during forward swimming

Olivia H. Hawkins[1,2]*, Victor M. Ortega-Jimenez[3], Chris P. Sanford[4]

[1]Department of Ecology, Evolution and Organismal Biology. Kennesaw State University, Kennesaw, GA

[2] Department of Biology, University of Louisiana at Lafayette, Lafayette, LA

[3] School of Chemical and Biomolecular Engineering. Georgia Institute of Technology, Atlanta, GA

[4] Research and Sponsored Programs, California State University, Northridge, CA

***Corresponding author:** ohawkins.research@gmail.com

Keywords: fish locomotion, swimming control, maneuverability, ribbon fin

SUMMARY STATEMENT

This study investigates turning in a knifefish and finds that the body, pectoral fins, and an elongated anal fin contribute to turning maneuvers.

ABSTRACT

Rapid turning and swimming contribute to ecologically important behaviors in fishes such as predator avoidance, prey capture, mating, and the navigation of complex environments. For riverine species, such as knifefishes, turning behaviors may also be important for navigating locomotive perturbations caused by turbulent flows. Most research on fish maneuvering focuses on fish with traditional fin and body morphologies, which primarily use body bending and the pectoral fins during turning. However, it is uncertain how fishes with uncommon morphologies, are able to achieve sudden and controllable turns. Here we studied the turning performance and the turning hydrodynamics of the Black ghost knifefish (*Apteronotus albifrons*, N=6) which has an atypical elongated ribbon fin. Fish were filmed while swimming forward at ~2 BL s^{-1} and feeding from a fixed feeder (control) and an oscillating

feeder (75 Hz) at two different amplitudes. 3D kinematic analysis of the body revealed the highest pitch angles and lowest body bending coefficients occurred during steady swimming. Low pitch angle, high maximum yaw angles and large body bending coefficients were characteristic of small and large turns. Asynchrony in pectoral fin use was low during turning, however ribbon fin wavelength, frequency, and wave speed were greatest during large turns. Digital particle image velocimetry (DPIV) showed larger counter-rotating vortex pairs produced during turning by the ribbon-fin in comparison to vortices rotating in the same direction during steady swimming. Our results highlight the ribbon fin's role in controlled rapid turning through modulation of wavelength, frequency, and wave speed.

1. INTRODUCTION

Fishes' turning maneuvers are commonly used during prey capture, predator avoidance, mating, or navigating complex environments (Webb, 1981). Turning during prey capture is especially important when pursuing evasive prey items (Domenici, 2001). For instance, after shooting prey with a jet of water, banded archer fish (*Toxotes jaculatrix*) turn rapidly to face and approach the quickly falling prey (Wöhl et al., 2007). Larval zebrafish (*Brachydanio rerio*) rely on routine turning maneuvers to approach and capture prey, but also produce quick large-angle turns as a form of an escape response when presented with a stimulus (Budick and O'Malley, 2000). Escape responses in the context of predator avoidance have been studied in many groups of fishes including sharks, bichirs, larval fishes, trout, and sunfishes and have direct fitness consequences (Webb, 1976; Webb, 1978a; Budick and O'Malley, 2000; Tytell and Lauder, 2002; Domenici et al., 2004; Gibb et al., 2006; Tytell and Lauder, 2008). An additional context in which turning has direct fitness consequences is during mating events. Some fish perform rapid turns during courting behavior such as the round belly cowfish (*Lactoria diaphanus*) in which the males rapidly and continually swim circles around the female who also turns to follow the male or flees (Moyer, 1979). Mating displays in high-backed pygmy swordtails (*Xiphophorus multilineatus*) also rely on turns in order for the male to showcase the vertical body bars on each side of its body to the female (Liotta et al., 2019). Finally, turning in the context of habitat navigation is shown to be especially important for fishes living in complex environments such as coral reefs (Gerstner, 1999). In freshwater systems, littoral ecomorphs of bluegill sunfish

(*Lepomis macrochirus*), which live amongst dense vegetation, have better performance while navigating an obstacle course in comparison to pelagic ecomorphs (Ellerby and Gerry, 2011). While turning is an important maneuver throughout a fish's life, there are still many species for which investigations of turning performance and kinematics are limited.

Most of what we know about the kinematics and hydrodynamics of routine turning maneuvers comes from fishes such as sunfish and trout that use the body and caudal fin to power steady swimming (Drucker and Lauder, 2001, 2002a; Lauder and Drucker, 2004). For these body undulating fishes, large normal forces produced by the body and caudal fin increase the momentum around the fish's center of mass thus aiding in turning maneuvers (Weihs, 1972). In addition to these surfaces, the median fins also play a role in turning in fishes. In bluegill sunfish, the dorsal and anal fins contribute part of the momentum needed to complete turns (Lauder and Drucker, 2004; Standen and Lauder, 2005; Tytell and Lauder, 2008). In brook trout (*Salvelinus fontinalis*), the anal fin plays more of a role in additive force generation with the caudal fin since the dorsal fin is more anterior (Standen and Lauder, 2007). Furthermore, brook trout use their pelvic fins to stabilize the body after turning (Standen, 2008). Similar to bluegill, bluefin tuna (*Thunnus thynnus)* and yellowfin tuna (*Thunnus albacares*) use the dorsal and anal fins to power turns in which the anterior dorsal fin is recruited for powering the turns and the posterior dorsal and anal fin are used to stabilize the body during the turn (Pavlov et al., 2017; Feng et al., 2020; Li, 2021). In addition to forces produced by the body, median and caudal fins, turning in sunfishes and trout is partly powered by imbalanced forces generated from asynchronous movements of the pectoral fins (Drucker and Lauder, 2002; Lauder and Drucker, 2004). In bluegill sunfish specifically, the pectoral fins are integral to maneuvering through complex environments even in the absence of traditional sensory cues (Flammang and Lauder, 2013). In fishes with rigid bodies such as the spotted boxfish (*Ostracion meleagris*), the pectoral fins are the primary control surfaces used for turning (Walker, 2000). Overall, body bending and the pectoral fins are the most commonly used surfaces for most bony fishes during turning maneuvers (Drucker and Lauder, 2001, 2002a).

While many fishes use body bending and the pectoral fins to turn, it is not known how fishes with uncommon fin morphologies perform turning maneuvers with non-traditional control surface such as the ribbon fin. The ribbon fin is present in multiple groups of fishes and can be found in dorsal, ventral, or dorso-ventral positions, driving swimming by producing waves

without body bending. Representatives of ribbon fin locomotion exist in multiple orders of both freshwater and marine fishes (Jagnandan and Sanford, 2013). Although the selective pressures on the evolution of ribbon finned fishes remains unknown, it has been suggested that swimming with an undulatory fin reduces mechanical and energetic costs while increasing maneuverability (Blake, 1983; Shirgoankar et al., 2008; Nevelen et al., 2013). Despite the implications of this fin for enhanced maneuverability, no study has investigated turning performance in a fish with a ribbon fin. This is surprising given that most ribbon-fin swimmers live in structurally and hydrodynamically complex habitats (e.g., coral reefs, vegetated streams).

One commonly studied ribbon fin swimmer is the weakly electric Black ghost knifefish, *Apteronotus albifrons* (Linnaeus, 1766). *A. albifrons* is one of 170 species of knifefish that swim using the gymnotiform mode (ventral ribbon fin propulsion) and inhabits the floodplains of the Amazon River which are dominated by heavy vegetation, macrophyte stems, and flooded forests (Crampton, 1996; Albert, 2001, Albert and Crampton, 2005). The extensive vegetation of these floodplains provides structural obstacles that increase habitat complexity and also cause complex flow patterns that can impact swimming performance (Ortega-Jimenez and Sanford, 2021). Beyond habitat navigation, turning also impacts foraging success. Apteronotids forage for small and active prey such as *Daphnia*, which require them to maneuver rapidly in order to feed (Nelson and MacIver, 1999). Similarly, African Knifefish, which also have an elongated ribbon fin, perform rapid turns to capture insect larva (Bleckmann, 1998). Since the ecology *A. albifrons* is not well understood, investigations focusing on maneuvering performance have implications for understanding constraints on habitat navigation and foraging in the presence of unpredictable flooding and drought conditions in the Amazon due to climate change (Katz et al., 2020).

To date, most research on the locomotion performance of *A. albifrons* has focused on steady swimming (Shirgoankar et al., 2008; Ruiz-Torres et al., 2013; Youngerman et al., 2014). Under laminar flow conditions, *A. albifrons* uses the ribbon fin to move linearly while maintaining a rigid body, therefore reducing potential disruption to its electrosensory system during prey detection (MacIver et al., 2010). Given the mechanical efficiency of ribbon fin locomotion, many studies have investigated steady swimming maneuvers computationally and through bioinspired Automated Underwater Vehicles (AUVs) (MacIver et al., 2004; Shirgoankar et al., 2008; Curet et al., 2011a; Neveln et al., 2013; Liu et al., 2018; English et al., 2019). All of these studies highlight how modulation of various parameters of the ribbon fin (i.e., curvature,

frequency, wavelength) impact forward swimming speed, backwards swimming, and hovering without consideration of the potential impact of traditional control surfaces such as the body and the pectoral fins. A recent study demonstrated that *A. albifrons* uses a combination of the body, pectoral fins, and the ribbon fin to navigate through unsteady flows (Ortega-Jimenez and Sanford, 2021). However, the contribution of these different control surfaces to turning maneuvers in steady flows, especially the ribbon fin, remains largely unexplored. Therefore, this study investigated the turning performance of *A. albifrons*, a fish with a non-traditional control surface, and its associated hydrodynamics. We used 3D kinematics to assess the contribution of the body, pectoral fins, and ribbon fin to steady swimming, small turns, and large turns while swimming forward. We also characterized the fluid dynamics of the wake produced by the ribbon fin during each maneuver. We predicted that the ribbon fin would contribute most to steady swimming, pectoral fins would dominate small turns, and that large turns would rely on all three control surfaces. This study specifically investigates the important role of the ribbon fin in eliciting small and large turns during forward swimming.

2. MATERIALS AND METHODS

2.1 Animal care and training

Six juvenile Black ghost knifefish (*Apteronotus albifrons;* Linneaus, 1766; 10.2 ± 0.86 cm) were obtained from local suppliers in Kennesaw, Georgia. Fish were housed separately in 151 L tanks containing dechlorinated freshwater. All tanks were maintained at 25-26 °C with a pH of 7-8. The aquatics facility maintained a 12 h: 12 h light: dark photoperiod. Fish received bloodworms *ad libitum*.

Prior to experiments, fish were trained to approach and follow an oscillating feeder under low flow conditions (~2 BL s^{-1}; See section 2.2). We used an oscillating feeder to establish three standardized treatments: steady forward swimming, small turns, and large turns. Fish received a week of training for all three treatments. For further details on training, see Ortega-Jimenez and Sanford (2021). Food was withheld 24 hours before experiments, and fish received a 30-minute acclimation period before filming. All fish performed all three treatments, and treatment order

was assigned at random. Husbandry and experiments adhered to Kennesaw State University IACUC (ACUP# 20-008).

2.2 Experimental design

Fish were filmed in a Brett-type 90L recirculating flow tank (Loligo Systems, Swim-90, Tjele, Denmark) with dechlorinated freshwater maintained at 25-26 °C. We used a single flow speed (15 cm s^{-1}: ~2 BL s^{-1}) to encourage forward swimming (Ortega-Jimenez and Sanford, 2021). The feeder (16 cm) was centered in the working section 8 cm from the bottom (70 x 20 x 20 cm; Fig. 1). We used the custom-built oscillating feeder to differentiate between treatments. It consisted of a feeding tube attached to the control arm of a waterproof 20 kg digital servo motor programmed by an Arduino Uno R3 microcontroller (ARDUINO, Italy; Fig. 1). The feeding tube was comprised of a small plastic cylinder with a 1 mm diameter hole in the center to hold bloodworms as described in Ortega-Jimenez and Sanford (2021). During steady swimming, the feeder remained stationary in the center of the working section. For the turning treatments, the feeder was programmed to oscillate at identical frequencies (0.75 Hz) but different angular amplitudes (30° and 45° respectively). For small turn treatments, one full oscillation of the feeder occurred over a horizontal distance of 8 cm at average speed of 3.1 cm s^{-1}. For large turn treatments, one full oscillation covered a horizontal distance of 14 cm at average speed of 4.7 cm s^{-1}.

2.3 Filming and digitization

We filmed at 250 fps (frames per second) using two synchronized Hi-Spec4 cameras (1696 x 1710 pixels; Fastec Imaging, San Diego, CA, USA). Cameras were placed lateral and ventral to the working section (Fig. 1). Cameras were calibrated using a 24-point calibration cube and the Direct Linear Transfer Method (DLT, version 7.1: Hedrick, 2008) for Matlab (Matlab 2020b, Mathworks, Natick, MA, USA). Sequences in which the fish swam for ~8 seconds behind the feeder or the fish completed a full turn to either the left or the right were retained for analysis. DLT software was also used to track the movement of the body, pectoral fins, and ribbon fin during steady swimming and turning using 14 digitized landmarks. Calibration and digitization code is available here: http://biomech.web.unc.edu/dltdv/. Representative video sequences of each treatment can be viewed in Movie 1.

Body landmarks were placed on the tip the of the snout, in between the pectoral fins, behind the pectoral fins, in the middle of the body, at the end of the ribbon fin attachment, and at the tip of the caudal fin. Pectoral fin landmarks were placed on the tip of the most distal fin ray and at the base of the fins. Ribbon fin landmarks were placed at the base of a fin ray at the center of the ribbon fin, on the distal end of the same fin ray, and on the tip of a distal fin ray located on the following wave crest. For additional information on landmarks see Fig. 2.

2.4 Kinematic measurements

For steady swimming, we analyzed sequences in which the fish had already approached the feeder and where the ribbon fin undulated for at least two cycles (N=6, 5-7 sequences per fish). For the small turn and large turn treatments, we analyzed sequences where the fish made a full turn to either the right or the left which was half of the total oscillation distance (small turn: N=6, 6-9 sequences per fish; large turn: N=6, 5-8 sequences per fish). The number of sequences analyzed for each individual for each treatment is located in Table S1. Kinematic variables detailed below were averaged for each fish and then averaged across all fish per treatment.

Variables of interest for the body consisted of pitch angle (°), maximum yaw angle (°), and the body bending coefficient ($ß_b$). Pitch angle was calculated as the angular orientation of the body in reference to a horizontal plane. Positive pitch angle indicated head up orientation of the body while negative pitch angle indicated head down orientation. We calculated yaw angle as the angular displacement of the body in the horizontal plane. The body bending coefficient, as described by Azizi and Landberg (2002), quantifies whole-body curvature. The coefficient is calculated as follows:

$$\beta_b = 1 - \frac{L_c}{L_b} \qquad (1.)$$

in which the distance between the snout and the end of the caudal fin (L_c) is divided by total body length (L_b) and subtracted from 1 (Fig. S1).

For the pectoral fins, we quantified pectoral fin flapping frequency (Hz), the dorso-ventral pectoral abduction angle (°), and the Asynchronous Index (AI). Pectoral flapping frequency and the dorso-ventral abduction angle were quantified using only the left pectoral fin as it was the only visible in both lateral and ventral views. Flapping frequency was calculated by tracking the tip of the left pectoral fin in the vertical plane throughout the sequence. The dorso-ventral abduction angle (°) was quantified as the angle formed between the body and the tip of

the left pectoral fin as it moved dorso-ventrally. The Asynchronous Index (AI) used in this study was adapted and modified from Gerry et al. (2008):

$$Asynchronous\ index(AI) = \sum \frac{\frac{x_{right}}{|x_{right}|} - \frac{x_{left}}{|x_{left}|}}{2(number\ of\ frames - 1)} \quad (2.)$$

in which AI is the sum of the ratios of the consecutive difference in x positions of the right pectoral fin to the absolute values of the same positions subtracted by the ratios of the difference in x positions of the left pectoral fin to the absolute value of those same positions all divided by two times the number of frames analyzed minus 1. This index is used to determine the percentage of the time the pectoral fins are moving in the same direction (synchronously) or different directions (asynchronously). AI values closer to one indicate the fins are moving asynchronously while values closer to 0 suggest synchronous movements of the fins.

Variables of interest for the ribbon fin included ribbon fin amplitude (°), frequency (Hz), wavelength (cm), and wave speed (cm s^{-1}). We defined amplitude as the stroke angle followed by the base and distal tip of a central fin ray, while frequency was the inverse period of the wave determined by the same two landmarks. We calculated wavelength as the distance between the tips of two consecutive wave crests. Wave speed was determined using the movement of a landmark at the distal tip of the fin ray at the middle of a wave crest and calculating the resulting first derivative of the MSE-quintic spline function (Walker, 1998; Ortega-Jimenez and Sanford, 2021). The MSE-quintic spline function smooths kinematic displacement data to reduce possible noise from digitization when calculating velocities and acceleration (Zin et al., 2020). See Ortega-Jimenez and Sanford (2021) for further details on the quantification of the ribbon fin variables.

2.5 Digital particle image velocimetry (DPIV) and analysis

Plastic particles (50 µm) were illuminated using a class-4 laser (Opto Engine LLC, Midvale, UT, USA; 532 nm, 5 W). The horizontal laser sheet was oriented approximately 1 cm below the oscillating feeder. Sequences were filmed at 500 fps^{-1} with a HiSpec 4 camera placed ventral to the working section of the flow tank (Fig. 1B). Two fish were used for DPIV analysis, and we filmed both fish performing all three treatments at a flow speed of 15 cm s^{-1} (~2BL s^{-1}). Sequences in which only the ribbon fin intersected the laser sheet were kept for analysis. We used PIVlab version 2.50 in Matlab for the analysis of time resolved paired images (Thielicke

and Stamhuis, 2014). Interrogation windows of 64 pixels^2 to 32 pixels^2 (50% step) were applied to all sequences and removed any vectors with standard deviations over 5. The resulting vorticity fields during the turning treatments were visually characterized and compared among steady swimming, small turn, and large turn treatments. We quantified the average vortex area for vortex pairs in each treatment using the 'Area Size' tool in PIVlab. Average vortex area (mm^2) consisted of values from both fish (steady swimming: n=14, small turn: n=22, large turn: n=14).

2.6 Statistical analysis

We used Repeated Measures ANOVA to determine the effect of treatment on the kinematic variables. For this analysis, we used the average values from each fish for each treatment. The Bonferroni pairwise comparison test served as post hoc analysis to assess significant differences between average values of the kinematic variables for steady swimming, small turns, and large turns. Normality assumptions were visually confirmed using QQ plots. Since we used a repeated measures design, we needed to verify that differences in the variation within-subjects among all possible combinations of the treatments remained equal. To test this assumption, we used Mauchly's test of sphericity which assumes that variation is equal when alpha > 0.05, and no violations of sphericity were detected. All data are presented as mean ± s.e. (standard error). Mean ± s.d. (standard deviation) is available in Table S2.

We used canonical discriminant analysis (CDA) as a multivariate approach to understand the contribution of the different body, pectoral fin, and ribbon fin variables to each of the investigated maneuvers following the approach of Youngerman et al. (2014). For this analysis, all observations for each fish for each treatment were used. We excluded the dorso-ventral pectoral abduction angle from analysis due to its inability to meet the homogeneity of covariance assumption. After visually confirming multivariate normality through QQ plots, all other variables were kept in the model. We used Wilk's lambda to assess the discriminant axes significantly contributing to the maximum separation of the treatments ($\alpha = 0.05$). R version 4.1.1 was used for all statistical analyses including the candisc (Friendly and Fox, 2021), nlme (Pinheiro et al., 2021) and stats packages (R Core Team, 2019).

3. RESULTS

3.1 Body kinematics

From steady swimming to large turns, the average pitch angle decreased significantly ($F_{2,10}$ =6.45, p = 0.02; Table S3, Fig. 3A). During steady swimming, the pitch angle was 6.16 ± 2.00 (°), almost double the pitch angle of fish during large turns (-6.45 ± 1.71 (°); Table 1). While pitch was significantly different between steady swimming and large turns (Bonferroni; t(5) = 3.78, p = 0.04; Table 1), there were no significant differences in pitch angle between steady swimming and small turns, or between small and large turns (Bonferroni; t(5) = 1.64, p = 0.49 and t(5) = 1.92, p = 0.34 respectively; Table 1). The average body bending coefficient varied significantly across treatments ($F_{2,10}$ = 43.22, p < 0.0001; Table S3, Fig. 3B). Significant differences in body bending coefficients were observed between steady swimming and large turns as well as between small and large turns (Bonferroni; t(5) = -7.91, p < 0.01 and t(5) = -5.93, p < 0.01 respectively; Table 1). The body bending coefficient during steady swimming was significantly lower that of small turns (Bonferroni; t(5) = -4.43, p = 0.02; Table 1). The average maximum yaw angle increased significantly across treatments ($F_{2,10}$ = 40.24, p < 0.0001; Table S3, Fig. 3C). Maximum yaw angle during large turns was nearly ten times than average maximum yaw during steady swimming, but not significantly higher than the yaw angle during small turns (Bonferonni; t(5) = 7.06, p = 0.003 and t(5) = 0.05, p = 0.15 respectively; Table 1).

3.2 Pectoral fin kinematics

Pectoral flapping frequency and dorso-ventral pectoral abduction angle were not found to significantly differ across treatments ($F_{2,10}$ = 0.36, p = 0.71 and $F_{2,10}$ = 0.64, p = 0.55 respectively; Table S3, Fig. 4A, B). The Asynchronous Index (AI) was found to differ significantly across treatments ($F_{2,10}$ =7.87, p < 0.01; Table S3, Fig. 4C). Average AI for the steady swimming treatment was 0.48 ± 0.02 and significantly larger than the AI during large turns (0.31 ± 0.04; Bonferroni; t(5) = 4.69, p = 0.02; Table 1). AI during steady swimming was higher than the AI for small turns but not significantly different (0.38 ± 0.04; Bonferroni; t(5) = 1.86, p = 0.37; Table 1). These results indicate that pectoral fins are moving asynchronously during all three treatments, but less asynchrony is occurring during large turns.

3.3 Ribbon fin kinematics

The average ribbon fin frequency differed significantly across treatments ($F_{2,10} = 5.35$, $p = 0.03$; Table S3, Fig. 5A). Ribbon fin frequency during large turns was significantly higher than the frequency during small turns but not steady swimming (Bonferroni; $t(5) = -3.89$, $p = 0.03$ and $t(5) = -2.57$, $p = 0.15$ respectively; Table 1). Like ribbon fin frequency, average wavelength differed significantly across treatments with frequency increasing from steady swimming to large turns ($F_{2,10} = 7.84$, $p = 0.009$; Table S3, Fig. 5B). Wavelength during small turns was 0.86 ± 0.15 cm which almost doubled the wavelength of the steady swimming treatment (Table 1). During large turns the wavelength was significantly higher than the wavelength during steady swimming (Bonferroni; $t(5) = -3.76$, $p = 0.04$; Table 1).

Average ribbon fin amplitude decreased from steady swimming to large turns, however treatment did not appear to have a significant effect ($F_{2,10} = 2.44$, $p = 0.14$; Table S3, Fig. 5C). Following in a similar pattern to ribbon fin frequency and wavelength, the average ribbon fin wave speed increased from steady swimming to large turns and differences were attributed to treatments ($F_{2,10} = 12.41$, $p < 0.01$; Table S3, Fig. 5D). Wave speed during small turns was significantly higher than the wave speed during steady swimming but not significantly lower than the wave speed during large turns (Bonferroni; $t(5) = -3.98$, $p = 0.03$ and $t(5) = -1.85$, $p = 0.37$ respectively; Table 1; Fig.5D). Wave speed for large turns was 8.14 ± 0.62 cm s^{-1} and tripled the average wave speed for steady swimming- therefore the means differed significantly (Bonferroni; $t(5) = -4.96$, $p = 0.01$; Table 1).

3.4 Canonical discriminant analysis

The first canonical axis had 97.49% discriminating power and therefore was the axis significantly contributing to the maximum separation of steady swimming, small turns, and large turns ($p < 0.05$; Table 2, Fig. 6). Ribbon fin wavelength, wave speed, ribbon fin frequency, pectoral fin flapping frequency, maximum yaw angle, and the body bending coefficient positively correlated with the first discriminant axis (Fig. 6). Asynchrony Index, ribbon fin amplitude, and pitch angle correlated negatively with the first axis (Fig. 6). Ribbon fin wavelength, wave speed, and amplitude as well as maximum yaw angle were positively correlated with the second discriminant axis while the Asynchrony Index, pitch angle, pectoral fin frequency, and the body bending coefficient correlated negatively (Fig. 6). For the first

canonical axis, the body bending coefficient, ribbon fin frequency, ribbon fin wavelength, and ribbon fin wave speed significantly contributed to the separation of treatments (Table S4). For the second canonical axis, pitch angle, the body bending coefficient, ribbon fin frequency, ribbon fin wavelength, and ribbon fin wave speed significantly contributed to the separation of treatments (Table S4).

3.5 Particle image velocimetry

In steady swimming sequences, we observed pairs of small counter rotating vortices (0.17 ± 0.036 mm^2) generated by the undulating ribbon-fin (Fig. 7A; Table S5). In the sequences for small turns, we found that the paired vortices still occurred, but the magnitude of these vortices had increased towards the center of the ribbon fin during the turn (Fig. 7B; Table S5). The largest vortex pairs were observed in the large turn treatment (Fig. 7C; Table S5). Vortices formed during large turns (0.32-0.92 mm^2) were 190% larger than those formed during steady swimming (0.1-0.23 mm^2). Vortices produced during small turns (0.18-0.65 mm^2) were 84% larger than those formed during steady swimming and 58% smaller than vortices formed during large turns. To further illustrate the hydrodynamics during turning, velocity profiles for each treatment can be found in Fig. S1.

4. DISCUSSION

Turning maneuvers in fishes are critical for survival and are involved in foraging, mating, and habitat navigation. Most investigations of turning in fishes focus on species with traditional control surfaces, while the mechanisms of turning in those with non-traditional control surfaces have been largely overlooked. To add to our understanding of turning in fish with non-traditional control surfaces, we investigated how the gymnotiform swimmer *A. albifrons* performs turning maneuvers using 3D kinematics and descriptive DPIV. Of the three control surfaces investigated (body, pectoral fins and ribbon fin) we expected that the ribbon fin would contribute most to steady swimming, pectoral fins would dominate during small turns, and all three control surfaces would be employed during large turns. We found that during steady swimming and turning maneuvers, *A. albifrons* recruited all three control surfaces, to differing degrees. Hydrodynamically, large turns are associated with an increase in vortex magnitude.

During steady swimming, individuals held their body in a slight head-up orientation, also noted previously in studies investigating forward swimming in *A. albifrons* (Ruiz-Torres et al., 2013; Youngerman et al., 2014; Ortega-Jimenez and Sanford, 2021). It has been suggested that positive pitch angles while swimming may be an effect of upward forces generated by the undulating ribbon fin (Ruiz-Torres, 2013). As the ribbon fin undulates during swimming, counter rotating vortices shed off the fin, causing downward momentum and a resulting heave force upwards (Shirgoankar et al., 2008; Curet et al., 2010). In the absence of additional control surfaces, *A. albifrons* may use the pectoral fins to mitigate body instability caused by heave forces. The Asynchronous Index (AI) during steady swimming was significantly higher than the AI during large turns and indicated that ~50% of the time the fins were used asynchronously during steady swimming (Table 1, Fig. 4C). Despite differences in AI, pectoral flapping frequency and pectoral dorso-ventral angle did not differ between steady swimming and the turning maneuvers (Table 1, Fig. Fig. 4A, B). In another ribbon fin swimmer, *Amia calva*, pectoral fin movements did not impact forward swimming speed, and it was suggested that pectoral movement may counterbalance the rotation around the fish's center of mass (Jagnandan and Sanford, 2013). It is possible that *A. albifrons* uses pectoral fins for stabilization rather than thrust generation during forward swimming similar to *A. calva*.

With the pectoral fins used for stabilization, the ribbon fin is thought to be the main contributor of forward swimming (Ortega-Jimenez and Sanford, 2021). Ribbon fin frequency, wavelength, and wave speed were lowest during steady swimming while ribbon fin amplitude was slightly larger although not significantly different from turning treatments (Table 1, Fig. 5). According to Youngerman et al. (2014), ribbon fin frequency during forward swimming is generally 4-6 Hz, which is also reflected our data (Table 1). Previous studies suggest modulation of frequency influences forward swimming speed, and this is one of the variables that significantly contributed to separating the treatments in the discriminant analysis (Jagnandan and Sanford, 2013; Youngerman et al., 2014; Ortega-Jimenez and Sanford, 2021; Table S4).

The body exhibited significantly more bending during the small and large turns when compared to steady swimming (Table 1). In addition, significantly higher maximum yaw angles were observed during turning (Table 1, Fig. 3B, C). Studies of *A. albifrons* suggest turning maneuvers in this species are rare and body bending is not common (Blake, 1983; MacIver et al., 2001; MacIver et al., 2010). However, in this study, *A. albifrons* clearly bend their bodies to

follow an oscillating feeder and Youngerman et al. (2014) observed body bending during free swimming maneuvers. These results also follow the observations of Ortega-Jimenez and Sanford (2021) in which *A. albifrons* bent its body in response to swimming downstream from an oscillating cylinder. Furthermore, Kasapi et al. (1993) also observed that body bending contributed to escape maneuvers in the African knifefish (*Xenomystus nigri*), which also swims using the gymnotiform mode. Given the frequency of turning in this study and in lab observations of *A. albifrons*, body bending appears to be common despite any potential negative impacts on the electro-sensory system. In this species, electro-receptors are located around the head, dorsal, and lateral surfaces to allow the fish to easily detect prey upstream (Nelson and MacIver, 1999). During foraging observations, and during turning maneuvers in this study, *A. albifrons* navigated with a head down (negative pitch) orientation (Nelson and MacIver, 1999). Maneuvering with a negative pitch angle may not only be behavioral, but a consequence of altering pectoral fin use to counter heave forces.

During small and large turns, there was no difference in flapping frequency or dorso-ventral abduction angle, but there was a difference in AI. While pectoral fin use can be considered asynchronous in all three treatments, asynchronous fin use was used ~30% of the time on average throughout large turns, ~38% during small turns, and ~48% during steady swimming (Table 1, Fig. 4C). We did not expect pectoral fin asynchrony to be lower during turning maneuvers when compared to forward swimming, but we have presented an alternative metric for asynchrony in this study (AI). Ortega-Jimenez and Sanford (2021) quantified fin asymmetry angles as a means of understanding asynchronous fin use, and these angles were highest when *A. albifrons* followed an oscillating cylinder. However, since AI considers timing of the maneuver in its calculation, it gives a glimpse of the temporal component of pectoral fin use. For instance, during turning, the inside fin initiated directional change, but through the remainder of the turn, both fins were held in similar positions (Video S1). Similarly, synchronous pectoral fin excursions were used to help power escape maneuvers in *X. nigri* (Kasapi et al., 1993). Synchronous pectoral fins movements may be used in tandem with acceleration of the ribbon fin to power turns, but we are restricted with our interpretation here as we did not measure acceleration in this study. However, Ortega-Jimenez and Sanford (2021) measured ribbon fin acceleration across different flow regimes, and considering the same flow

speed (1.8 BL s^{-1}), acceleration increased from 45 cm s^{-1} in laminar flow to 484 cm s^{-1} when the fish actively followed an oscillating cylinder.

Ribbon fin wavelength was similar between small and large turns and contributed significantly to turning (Table 1; Fig. 5B; Table S3). Since it is suggested that *A. albifrons* has active control over fin ray curvature, and larger wavelengths increase the surface area of the fin for fluid loading, active modulation of the ribbon fin appears to drive turning (Youngerman et al., 2014). Ribbon fin wave speed may also contribute to amount of thrust that can be generated from fluid loading, which was supported by the observation that large turns were characterized by a significant increase in wave speed (Table 1; Fig. 5D). As previously mentioned, the ribbon fin generates heave forces which may grow in magnitude as wave speed increases thus contributing to torque around the fish's center of mass which would explain the negative pitch angle observed during turning (Fig. 3A).

In addition to the kinematic analysis, the hydrodynamic analysis suggests the ribbon fin is a major contributor to turning maneuvers. We observed that vortex size greatly increases from small turns to large turns, and previous analysis of the ribbon fin wake as *A. albifrons* followed an oscillating cylinder showed similar patterns (Fig. 7, Ortega-Jimenez and Sanford, 2021). It is unclear whether instantaneous increases in wave speed during turning would result in in higher energetic costs as it is not known if the whole fin is under active or passive control. Increased understanding of the extent to which *A. albifrons* controls different parts of the fin will increase our current understanding of the potential metabolic costs of gymnotiform swimming. It should be noted that our DPIV measurements only take into account the contribution of the ribbon fin. Previous work on knifefish swimming in perturbed flows suggest that the ribbon fin has a major contribution on thrust production, while the pectoral fins are used for swimming control (Ortega-Jimenez and Sanford, 2021). Future work that includes the hydrodynamics of pectoral fins will provide a more complete understanding of their role in turning performance.

In the broader context of fish evolution, this study highlights the need to expand our knowledge of the contribution of alternate control surfaces to ecologically relevant maneuvers such as turning. Specifically, future studies would benefit from the investigation of other ribbon-fin swimmers where the anatomical placement and morphology of the ribbon fin differs from that of *A. albifrons* to gain a more comprehensive understanding of selective pressures associated with ribbon-fin swimming. Beyond biology, the results of these types of

investigations can be applied to current models of ribbon fin inspired Automated Underwater Vehicles (AUV's) (MacIver et al., 2004; Curet et al., 2011a, Neveln et al., 2013). In the case of *A. albifrons* and other gymnotid knifefishes in the Amazon that are facing increasingly unpredictable water levels in their habitats, understanding maneuvering performance may inform ecologists of the potential spatial constraints of these species. In structurally complex habitats like the Amazon, low water (decreased volume) regimes reduce the amount of open space for navigation in between flood plains and river systems which may hinder foraging, mating, and seasonal migrations in certain fish assemblages (Fernandes, 1997; Silva et al., 2021).

In conclusion, we highlight the important contribution of a non-traditional control surface to turning maneuvers in a gymnotiform swimmer. The kinematics data suggest that the ribbon fin is recruited heavily during turning, with body bending and pectoral fin movements contributing to changes in heading and stabilization. Our descriptive hydrodynamics data shows that vortices during turning are larger than those during steady swimming. Future studies should investigate maneuvering in other ribbon fin swimmers to further understand the convergence of this swimming mode, inspire more maneuverable AUV's, and to further understand the ecomorphological implications of the ribbon fin.

ACKNOWLEDGEMENTS

The authors would like to thank Dante Orlando for assistance in building and programming the oscillating feeder and Ashlyn Stanalonis for help with filming and fish care. The authors also thank two anonymous reviewers for their insightful comments on the manuscript.

REFERENCES

Albert, J.S. (2001). Species diversity and phylogenetic systematics of American knifefishes (Gymnotiformes, Teleostei). *Misc. Publ. Mus. Zool*. Univ. Michigan **190**, 1–127.

Albert, J.S., Crampton, W.G.R. (2005). Diversity and phylogeny of Neotropical electric fishes (Gymnotiformes). In *Electroreception* (ed. R.R. Fay, A.N. Popper, T.H. Bullock, C.D. Hopkins), pp.360-409. Springer Handbook of Auditory Research, vol. 21. New York: Springer Publishing.

Aziz, E. and Landberg, T. (2002). Effects of metamorphosis on the aquatic escape response of the two-lined salamander (*Eurycea bislineata*). *J. Exp. Biol*. **205**, 841–849.

Blake, R.W. (1983) Swimming in the electric eels and knifefishes. *Can. J. Zool.* 61, 1432–1441.

Budick, S.A. and O'Malley, D.M. (2000). Locomotor Repertoire of the Larval Zebrafish: Swimming, Turning and Prey Capture. *J. Exp. Biol*. **203**, 2565-2579.

Crampton, W.G.R. (1996). Gymnotiform fish: an important component of Amazonian floodplain fish communities. *J. Fish. Biol*. **48**, 298-301.

Curet, O. M., AlAli, I. K., MacIver, M. A., Patankar, N. A. (2010). A versatile implicit iterative approach for fully resolved simulation of self-propulsion. *Comput. Methods Appl. Mech. Eng.* 199, 2417-2424.

Curet, O.M., Patankar, N.A., Lauder, G.V., MacIver, M.A. (2011a) Aquatic maneuvering with counter-propagating waves: a novel locomotive strategy. *J. R. Soc. Interface*. **8**, 1041–1050.

Domenici, P. (2001). The scaling of locomotor performance in predator-prey encounters: from fish to killer whales, *Comp. Biochem. Physiol. A.* **131**,169-82.

Domenici, P., Standen, E.M., Levine, R.P. (2004). Escape manoeuvres in the spiny dogfish (*Squalus acanthias*). *J. Exp. Biol.* **207**(13), 2339-49.

Drucker, E.G., and Lauder, G.V. (2001). Wake dynamics and fluid forces of turning maneuvers in sunfish. *J. Exp. Biol*. **204**, 431-442.

Drucker, E.G. and Lauder, G.V. (2002a) Wake Dynamics and Locomotor Function in Fishes: Interpreting Evolutionary Patterns in Pectoral Fin Design. *Intgr. Comp. Biol*. **42**, 997–1008.

Emde G, h. (1998). Finding food: senses involved in foraging for insect larvae in the electric fish *Gnathonemus petersii*. *J Exp Biol*. **7**, 969-80.

Ellerby, D.J., Gerry, S.P. (2011). Sympatric divergence and performance trade-offs of bluegill ecomorphs. *Evol. Biol.* **38**, 422–433.

Feng, Y.K., Liu, H.X., Su, Y.Y., Su, Y.M. (2020). Numerical study on the hydrodynamics of C-turn maneuvering of a tuna-like fish body under self-propulsion. *J. Fluids Struct*. **94**, doi: https://doi.org/10.1016/j.jfluidstructs.2020.102954.

Fernandes, C. C. (1997). Lateral migration of fishes in Amazon floodplains. *Ecol. Fresh. Fish*, **6**, 36–44. doi: https://doi.org/10.1111/j.1600-0633.1997.tb00140.x.

Flammang, B. E., and Lauder, G.V. (2013). Pectoral Fins Aid in Navigation of a Complex Environment by Bluegill Sunfish Under Sensory Deprivation Conditions. *J. Exp. Biol*. **216**: 3084–3089. doi: https://doi.org/10.1242/jeb.080077.

Friendly, M., Fox, J. (2021). *candisc: Visualizing Generalized Canonical Discriminant and Canonical Correlation Analysis*. R package version 0.8-6, https://CRAN.R-project.org/package=heplots.

Gerry, S. P., Ramsay, J. B., Dean, M. N., & Wilga, C. D. (2008). Evolution of asynchronous motor activity in paired muscles: effects of ecology, morphology, and phylogeny. *Integr. Comp. Biol., 48(2), 272–282.* doi: https://doi.org/10.1093/icb/icn055.

Gerstner, C.L. (1999). Maneuverability of four species of coral-reef fish that differ in body and pectoral fin morphology. *Can. J. Zoo*. **77**: 1102-1110.

Gibb, A.C., Swanson, B.O., Wesp, H., Landels, C., Liu, C. (2006). Development of the escape response in teleost fishes: do ontogenetic changes enable improved performance? *Physiol. Biochem. Zool.* **79**(1), 7-19.

Hedrick, T.L. (2008). Software techniques for two- and three-dimensional kinematic measurements of biological and biomimetic systems. *Bioinsp. Biomim*. **3**, 034001.

Jagnandan K., and Sanford, C.P. (2013). Kinematics of ribbon-fin locomotion in the bowfin, *Amia calva*. *J. Exp. Zool. A*. **319**, 569–83.

Kasapi, M. A., Domenici, P. D., Blake, R. W., Harper, D. G. (1993). The kinematics and performance of escape responses of the knifefish *Xenomystus nigri*. *Can. J. Zool*. **71**, 189–195.

Katz, E., Lammel, A., Bonnet, M.P. (2020) Climate Change in a Floodplain of the Brazilian Amazon: Scientific Observation and Local Knowledge. In: Welch-Devine M., Sourdril A., Burke B. (eds) *Changing Climate, Changing Worlds.* Ethnobiology. Springer, Cham. doi: https://doi.org/10.1007/978-3-030-37312-2_7.

Lauder, G.V., and Drucker, E.G. (2004). Morphology and experimental hydrodynamics of fish fin control surfaces. *IEEE J. Ocean. Eng*. **29**, 556–571.

Li, X. (2021). Hydrodynamic Analysis for the Morphing Median Fins of Tuna during Yaw Motions, *App. Bionics Biomech*. 6630839. doi: https://doi.org/10.1155/2021/6630839.

Liotta, M.N., Abbott, J.K., Rios-Cardenas, O., Morris, M.R. (2019). Tactical dimorphism: the interplay between body shape and mating behaviour in the swordtail *Xiphophorus multilineatus* (Cyprinodontiformes: Poeciliidae), *Biol. J. Linn. Soc.* **127**(2), 337–350.

Liu, H. and Curet, O.M. (2018). Swimming performance of a bio-inspired robotic vessel with undulating fin propulsion. *Bioinsp. Biomim*. **13**, 056006.

MacIver, M. A., Fontaine, E., Burdick, J. W. (2004). Designing future underwater vehicles: principles and mechanisms of the weakly electric fish. *IEEE J. Oceanic Eng*. **29**, 651-659.

MacIver, M.A., Sharabash, N.M., Nelson, M.E. (2001) Prey-capture behavior in gymnotid electric fish: Motion analysis and effects of water conductivity. *J. Exp. Biol.* **204**, 543–557.

MacIver, M.A., Patankar, N.A., Shirgaonkar, A.A. (2010) Energy-Information Trade-Offs between Movement and Sensing. *PLoS Comput Biol* **6**(5), e1000769.

Moyer, J. T. (1979). Mating strategies and reproductive behaviour of ostraciid fishes at Miyake-Jima, Japan. *Jap. J. Ichthyol*. **26**, 148-160.

Nelson, M.E., and MacIver, M.A. (1999). Prey capture in the weakly electric fish *Apteronotus albifrons*: sensory acquisition strategies and electrosensory consequences. *J. Exp. Biol*. **202** (10): 1195–1203. doi: https://doi.org/10.1242/jeb.202.10.1195.

Neveln, I.D., Bai, Y., Snyder, J.B., Solberg, J.R., Curet, O.M., Lynch, K.M., MacIver, M.A. (2013). Biomimetic and bio-inspired robotics in electric fish research. *J. Exp. Biol.* **216**, 2501–2514.

Ortega-Jimenez, V.M., and Sanford, C.P. (2021). Beyond the Kármán Gait: Knifefish swimming in periodic and irregular vortex streets. *J. Exp. Bio.* doi: https://doi.org/10.5061/dryad.sqv9s4n37.

Pavlov, V., Rosental, B., Hansen, N.F., Beers, J., Parish, G. (2017). Hydraulic control of tuna fins: A role for the lymphatic system in vertebrate locomotion. *Science***. 357**(6348), 310–314.

Pinheiro, J., Bates, D., DebRoy, S., Sarkar, D., R Core Team (2021). *nlme: Linear and Nonlinear Mixed Effects Models*. R package version 3.1-153, https://CRAN.R-project.org/package=nlme.

R Core Team. (2014). R: A language and environment for statistical computing. R Foundation for Statistical Computing, Vienna, Austria. URL http://www.R-project.org/.

Ruiz-Torres, R., Curet, O.M., Lauder, G.V., MacIver, M.A. (2013). Kinematics of the ribbon fin in hovering and swimming of the electric ghost knifefish. *J. Exp. Biol*. **216**, 823–834.

Shirgaonkar, A.A., Curet, O.M., Patankar, N.A., MacIver, M.A. (2008). The hydrodynamics of ribbon-fin propulsion during impulsive motion. *J. Exp. Biol*. **211**, 3490–3503.

Silva, P.B., Arantes, C.C., Freitas, C.E.C., Petrere, M., Ribeiro, F.R.V. (2021). Seasonal hydrology and fish assemblage structure in the floodplain of the lower Amazon River. *Ecol Freshw Fish*. **30**: 162– 173. https://doi.org/10.1111/eff.12572.

Standen, E.M. (2008). Pelvic fin locomotor function in fishes: three-dimensional kinematics in rainbow trout (*Oncorhynchus mykiss*). *J. Exp. Biol*. **211**: 2931–2942. doi: https://doi.org/10.1242/jeb.018572.

Standen, E. M., and Lauder, G.V. (2005). Dorsal and Anal Fin Function in Bluegill Sunfish *Lepomis Macrochirus*: Three-Dimensional Kinematics During Propulsion and Maneuvering. *J. Exp. Biol.* **208**: 2753–2763. doi: https://doi.org/10.1242/jeb.01706.

Standen, E. M., and Lauder, G.V. (2007). Hydrodynamic Function of Dorsal and Anal Fins in Brook Trout (*Salvelinus Fontinalis*). *J. Exp. Biol.* **210**: 325–339. doi: https://doi.org/10.1242/jeb.02661.

Thielicke, W., Stamhuis, E.J. (2014). PIVlab – Towards User-friendly, Affordable and Accurate Digital Particle Image Velocimetry in MATLAB. *J. Open Res. Soft.* **2**(1): e30. doi: https://doi.org/10.5334/jors.bl.

Tytell, E.D., and Lauder, G.V. (2002). The C-start escape response of *Polypterus senegalus*: bilateral muscle activity and variation during stage 1 and 2. *J. Exp. Biol.* **205**, 2591-603.

Tytell, E.D., and Lauder, G.V. (2008). Hydrodynamics of the escape response in bluegill sunfish, *Lepomis macrochirus*. *J. Exp. Biol*. **211**:3359-3369. doi: https://doi.org/10.1242/jeb.020917.

Walker, J.A. (1998). Estimating velocities and accelerations of animal locomotion: a simulation experiment comparing numerical differentiation algorithms. *J. Exp. Biol*. **201**, 981 -995.

Walker, J.A. (2000) Does a rigid body limit maneuverability? *J. Exp. Biol*. **203**, 3391-3396.

Webb, P. W. (1976). The effect of size on the fast-start performance of rainbow trout *Salmo gairdneri* and a consideration of piscivorous predator–prey interaction. *J. Exp. Biol*. **65**, 157–177.

Webb, P. W. (1978a). Fast-start performance and body form in seven species of teleost fish. *J. Exp. Biol.* **74**, 211–226.

Webb, P.W. (1981). Composition and mechanics of routine swimming of rainbow trout, *Oncorhynchus mykiss*. *Can. J. Fish. Aquat. Sci*. **48**, 583-590.

Weihs, D. (1972). A hydrodynamical analysis of fish turning maneuvers. *Proc. R. Soc. B*. **182**, 69-72.

Wöhl, S. and Schuster, S. (2007). The predictive start of hunting archer fish: a flexible and precise motor pattern performed with the kinematics of an escape C-start. *J. Exp. Biol.* **210**, 311-24)

Youngerman, E. D., Flammang, B.E., Lauder, G.V. (2014). Locomotion of free-swimming ghost knifefish: anal fin kinematics during four behaviors. *Zool*. **117**, 337-348.

Zin, M.A.M., Rambely, A.S., Ariff, N.M., Ariffin, M.S. (2020). Smoothing and Differentiation of Kinematic Data Using Functional Data Analysis Approach: An Application of Automatic and Subjective Methods. *Appl. Sci*. **10**(7):2493. doi: https://doi.org/10.3390/app10072493.

Competing interests

No competing interests declared.

Code availability

Code for digitization used in this study is available at https://biomech.web.unc.edu/dltdv/. Code supporting DPIV analysis can be found here: https://pivlab.blogspot.com/2017/07/pivlab-direct-download.html.

Data availability

Datasets have been made available using Data Dryad at the following link: https://doi.org/10.5061/dryad.9ghx3ffhj.

Ethics statement

Experiments and husbandry protocols were approved by Kennesaw State University's Institutional Animal Care and Use Committee (ACUP #20-008) and followed federal guidelines and regulations. No fish were sacrificed for the purposes of this study.

Funding

This work was supported by the College of Science and Mathematics at Kennesaw State University [C.P.S.].

Figures

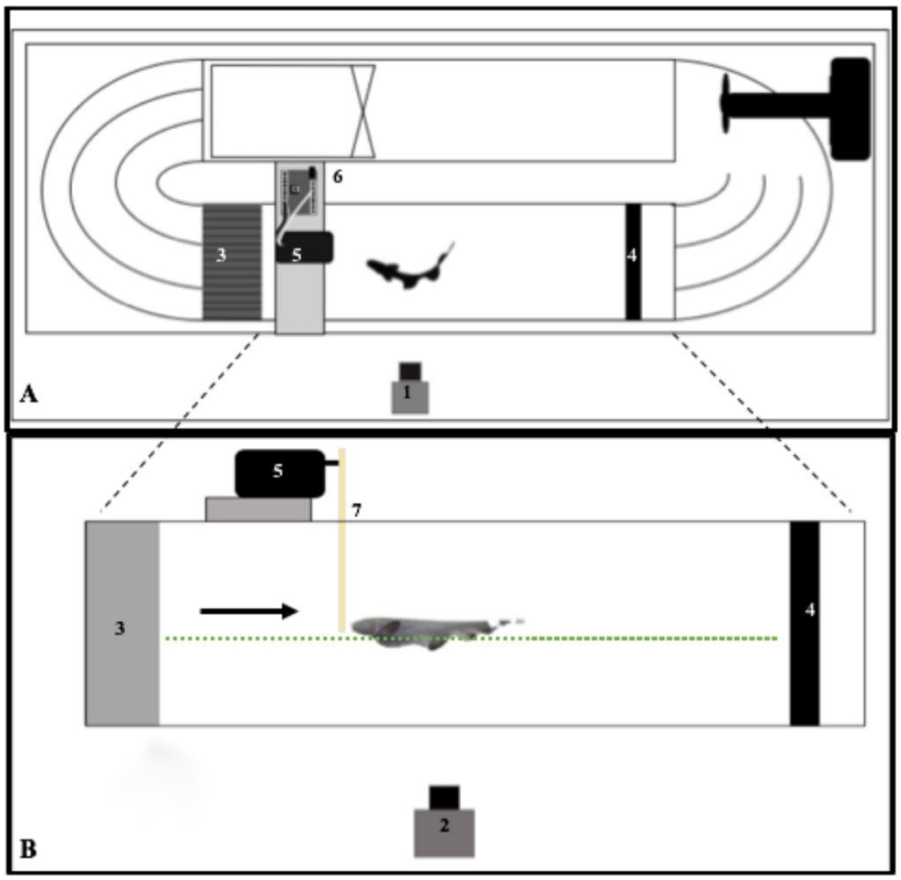

Figure 1. Experimental set-up. Experimental set-up of the flow tank including the aerial view (A) and lateral view (B). Cameras were placed lateral (1) and ventral (2) to the working section of the flow tank. A flow rectifier (3) and mesh (4) were placed upstream and downstream of the working section respectively. The oscillating feeder was placed in the center of the working section and consisted of a digital servo motor (5) programed by an Arduino Uno R3 microcontroller (6) with an attached feeder (7). The black arrow indicates the direction of flow (BL s^{-1}), and the green dotted line shows the location of the laser sheet used for digital particle image velocimetry (DPIV). Schematic not drawn to scale.

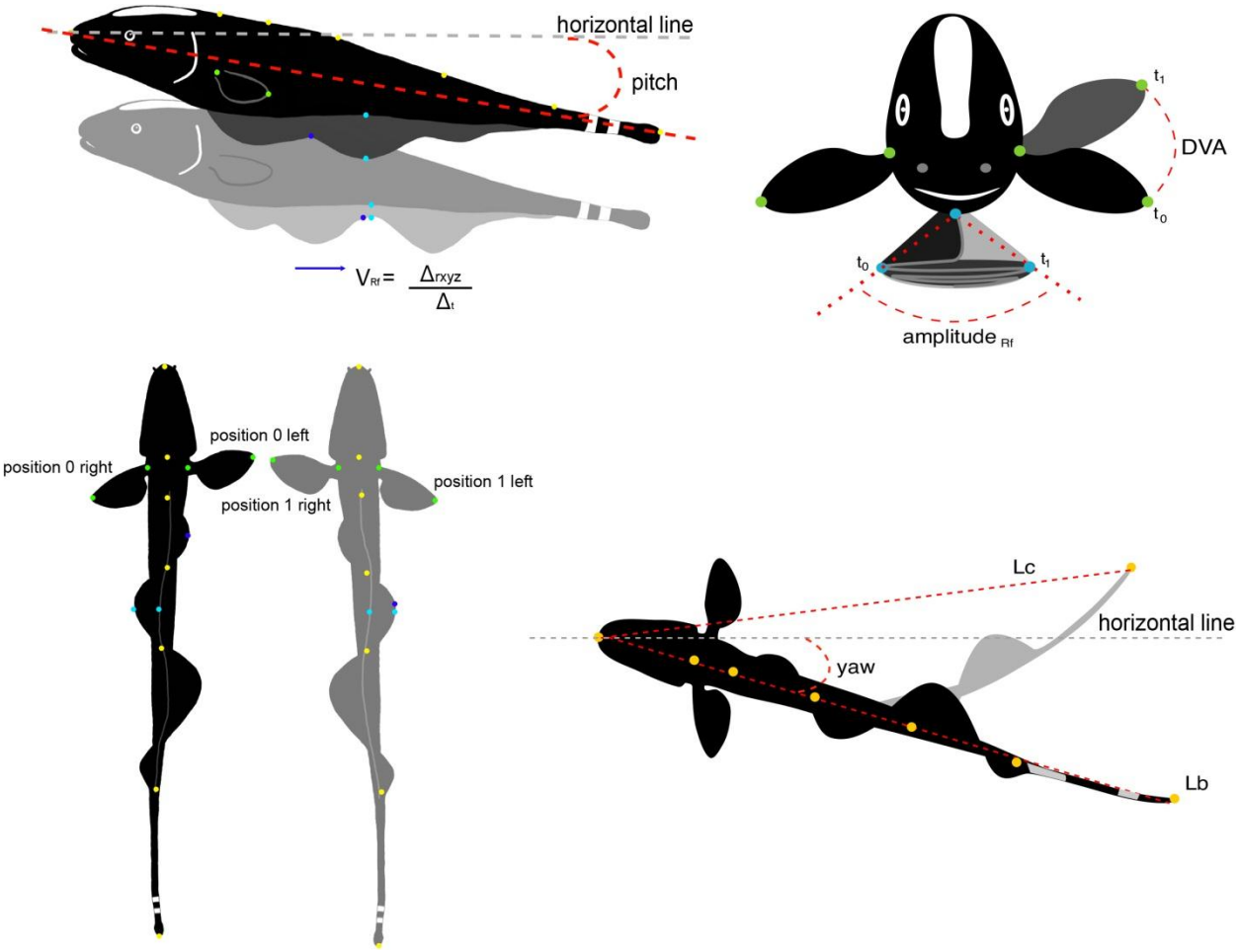

Figure 2. Digitization landmarks. Schematic of the 14 digitized landmarks used in the calculation of pitch angle, maximum yaw angle, body bending coefficient, dorso-ventral pectoral fin abduction angle (DVA), Asynchronous Index (AI), pectoral fin flapping frequency, ribbon fin amplitude, ribbon fin wavelength, and ribbon fin wave speed. Yellow points represent body points, green points represent pectoral fin points, light blue points represent fixed ribbon fin points, and the dark blue point represents a moving ribbon fin point. See section 2.3 and 2.4 of the methods for detailed information on each variable. Figure reproduced and modified from Ortega-Jimenez and Sanford (2021).

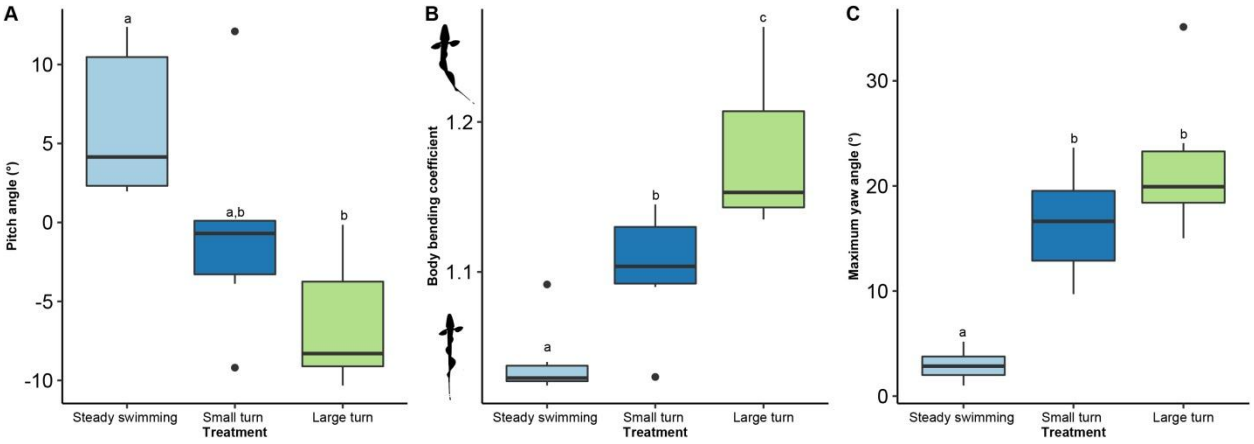

Figure 3. Body kinematics results. Pitch angle (A), yaw angle (B), and the body bending coefficient (C) by treatment (*n=6*). Solid lines in the boxplots represent the median value of the variable while whiskers represent the minimum and maximum values. Letters indicate results of Bonferroni p-value adjustments following a One-Way Repeated Measures ANOVA (α = 0.05).

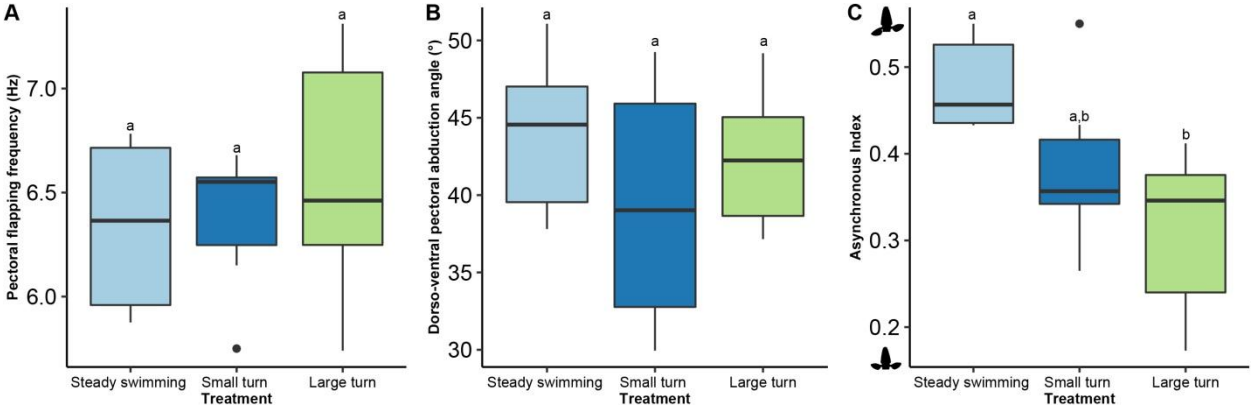

Figure 4. Pectoral fin kinematics results. Averages for pectoral fin flapping frequency (A), dorso-ventral pectoral abduction angle (B), and the Asynchronous Index (C) by treatment (*n=6*). Solid lines in the boxplots represent the median value of the variable while whiskers represent the minimum and maximum values. Letters indicate results of Bonferroni p-value adjustments following a One-Way Repeated Measures ANOVA (α = 0.05).

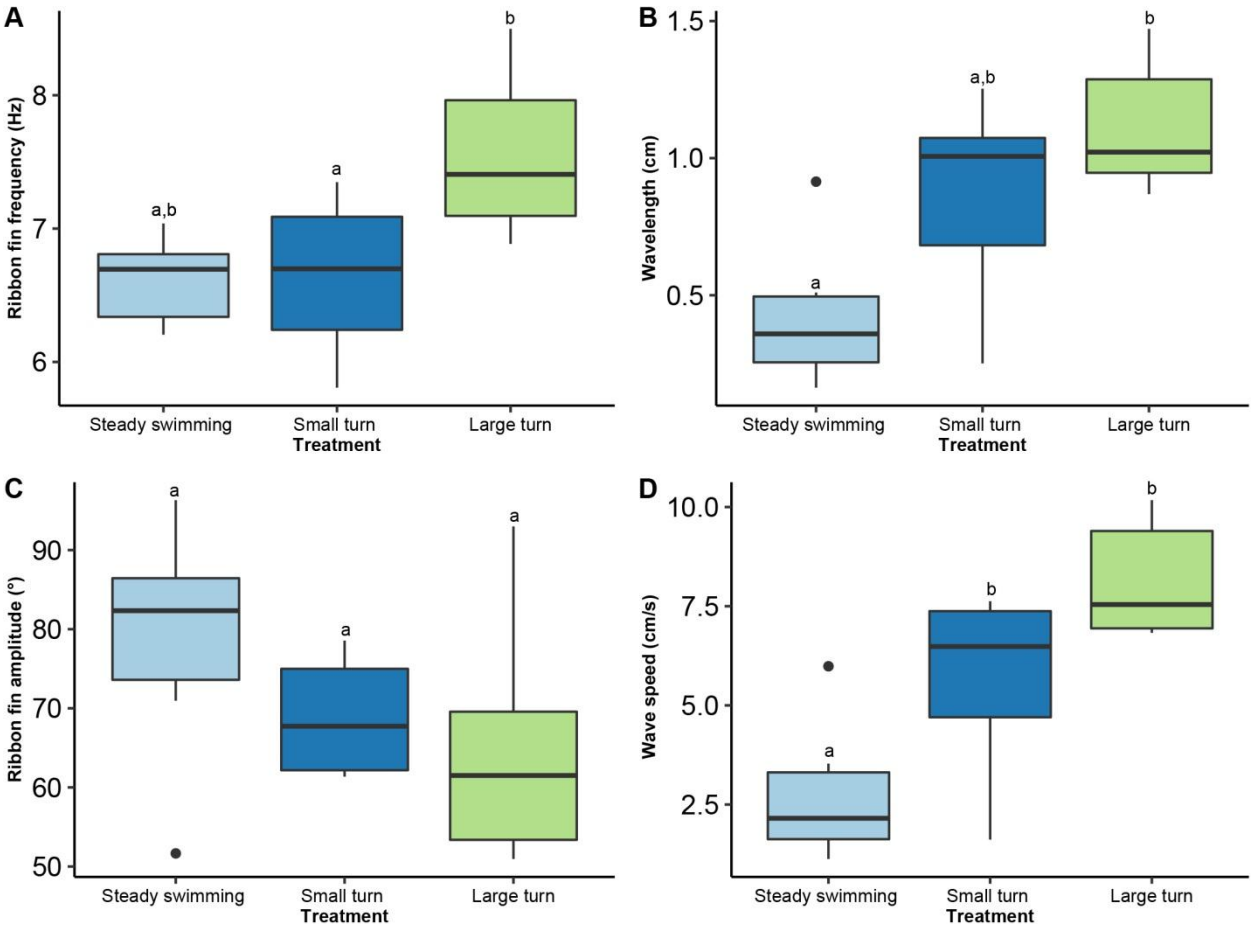

Figure 5. Ribbon fin kinematics results. Averages for ribbon fin frequency (A), wavelength (B), ribbon fin amplitude (C), and wave speed (D) by treatment (*n=6*). Solid lines in the boxplots represent the median value of the variable while whiskers represent the minimum and maximum values. Letters indicate results of Bonferroni p-value adjustments following a One-Way Repeated Measures ANOVA ($\alpha = 0.05$).

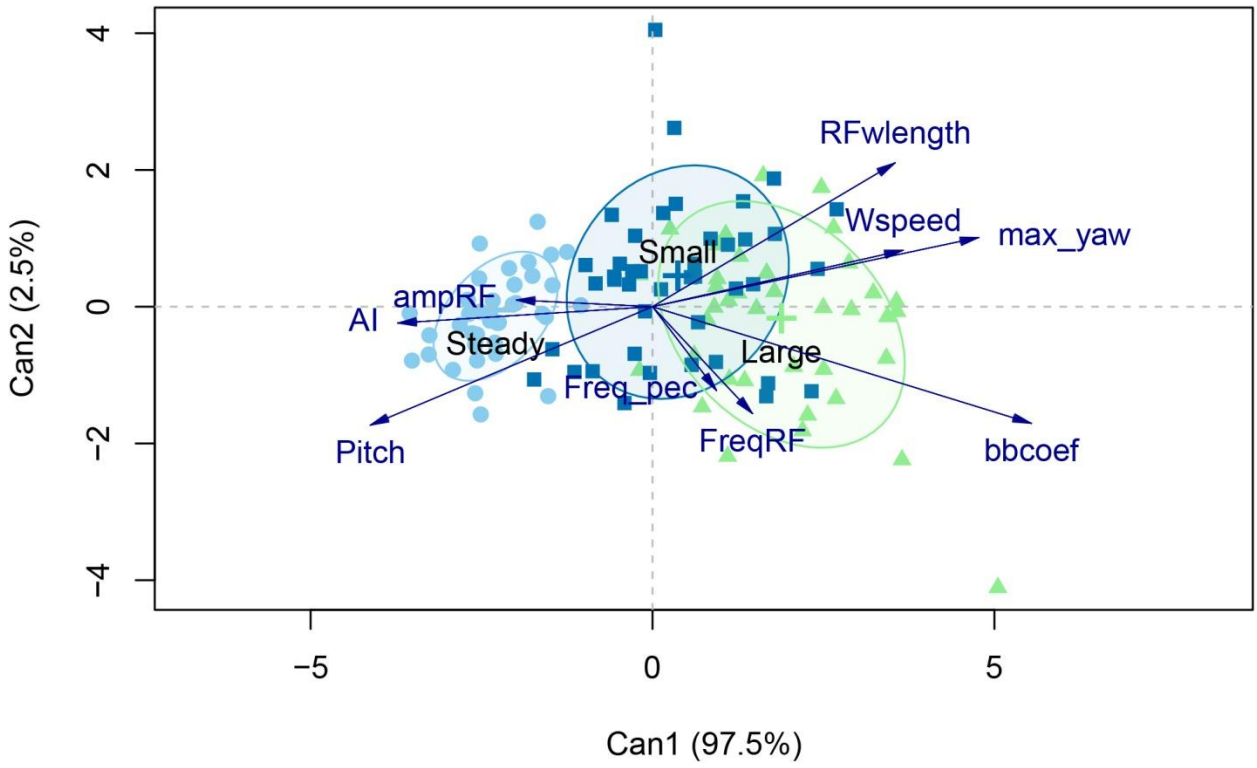

Figure 6. Canonical discriminant analysis (CDA) for steady swimming, small turns, and large turns. Canonical scores are represented by light blue circles for steady swimming, dark blue squares for small turns, and green triangles for large turns. Crosses represent canonical means, and are surrounded by 68% probability ellipses. Kinematic variables included in the analysis are pitch angle, body bending coefficient (bbcoef), maximum yaw angle (yaw_max), asynchronous index (AI), pectoral flapping frequency (Freq_pec), ribbon fin amplitude (ampRF), ribbon fin wavelength (RFwlength), ribbon fin frequency (FreqRF), and wave speed (Wspeed).

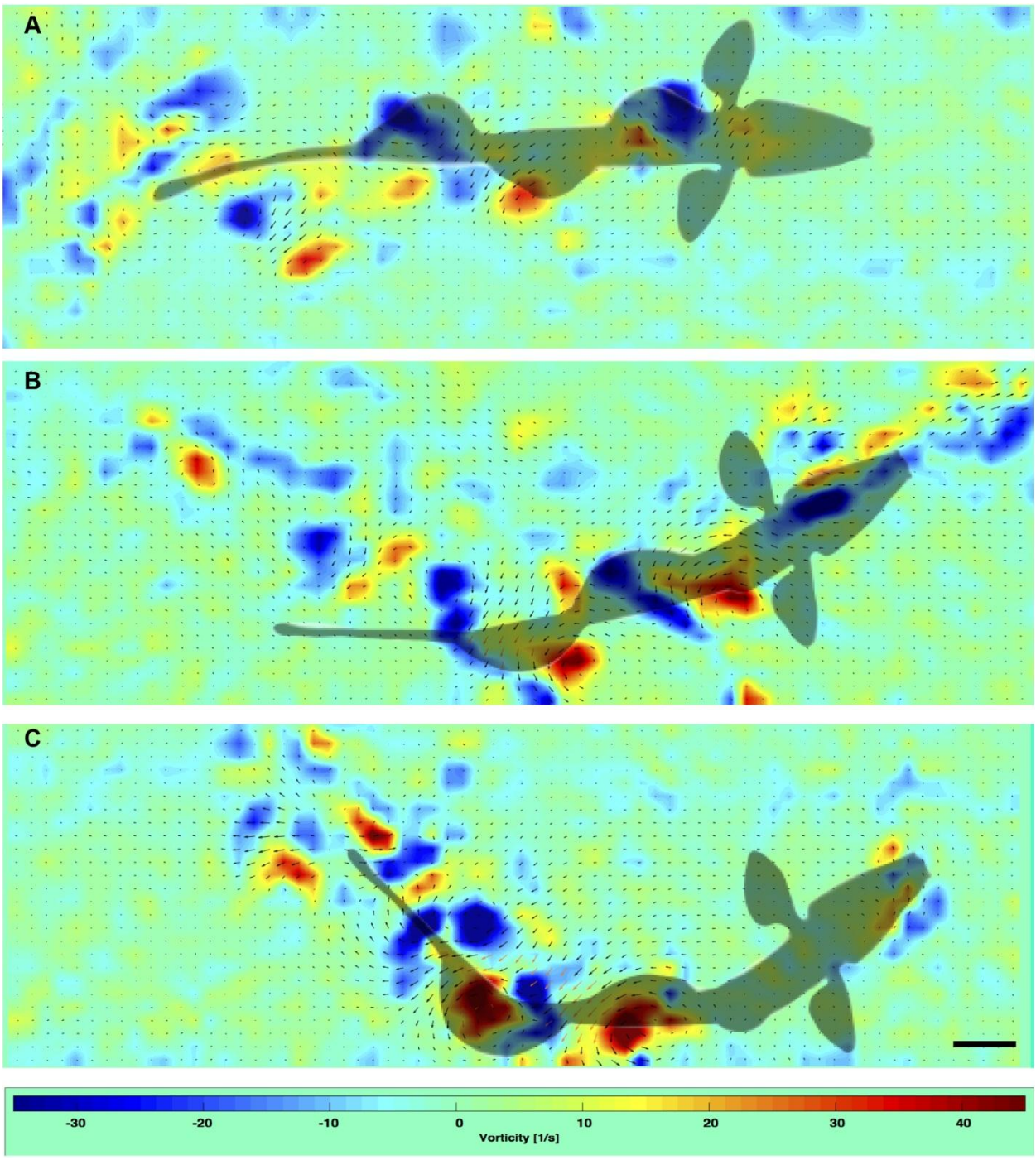

Figure 7. Fluid dynamics of the ribbon fin during steady swimming and turning maneuvers. Vorticity fields (s^{-1}) representing steady swimming (A), small turn (B), and large turn treatments (C). Fish silhouettes show the relative location of the fish with the ribbon fin intersecting the laser sheet. Scale bar represents 1 cm.

Table 1. Kinematic variables for the body, pectoral fins, and ribbon fin. Results of kinematic measurements for each maneuver performed by *Apteronotus albifrons* (N=6). Results are reported here as mean ± s.e. (standard error) using the means of all individuals during steady swimming, small turns, and large turns. Superscript letters correspond to statistical significance among maneuvers determined by adjusted p-values from Bonferroni pairwise comparison tests following a One-Way Repeated Measures ANOVA ($\alpha = 0.05$).

Kinematic variable	Steady Swimming	Small maneuver	Large maneuver
Pitch angle (°)	6.16 ± 2.00^{a}	$-0.38 \pm 2.87^{a,b}$	-6.45 ± 1.71^{b}
Maximum yaw angle (°)	2.95 ± 0.61^{a}	16.5 ± 2.11^{b}	22.1 ± 2.89^{b}
Body bending coefficient	1.04 ± 0.01^{a}	1.10 ± 0.02^{b}	1.17 ± 0.02^{c}
Pectoral fin flapping frequency (Hz)	6.34 ± 0.17^{a}	6.38 ± 0.15^{a}	6.57 ± 0.23^{a}
Dorso-ventral pectoral angle (°)	43.95 ± 2.15^{a}	39.35 ± 3.30^{a}	42.37 ± 1.89^{a}
Asynchronous Index	0.48 ± 0.02^{a}	$0.38 \pm 0.04^{a,b}$	0.31 ± 0.04^{b}
Ribbon fin frequency (Hz)	$6.62 \pm 0.14^{a,b}$	6.64 ± 0.25^{a}	7.56 ± 0.26^{b}
Ribbon fin amplitude (°)	78.52 ± 6.34^{a}	68.85 ± 3.08^{a}	64.98 ± 6.55^{a}
Ribbon fin wavelength (cm)	0.43 ± 0.11^{a}	$0.86 \pm 0.15^{a,b}$	1.11 ± 0.10^{b}
Ribbon fin wave speed (cm s^{-1})	2.76 ± 0.73^{a}	5.66 ± 0.96^{b}	8.14 ± 0.62^{b}

Table 2. Canonical discriminant analysis (CDA) axes results. Points represent individual observations from six individuals for steady swimming, small turns, and large turns. An axis significantly contributes to maximum linear separation of groups when $p < 0.05$.

Discriminant axis	Eigenvalue	Percent	Correlation	Wilk's Lambda	Probability
1	3.03	97.49	0.75	0.23	< 0.0001
2	0.08	2.51	0.07	0.93	0.40

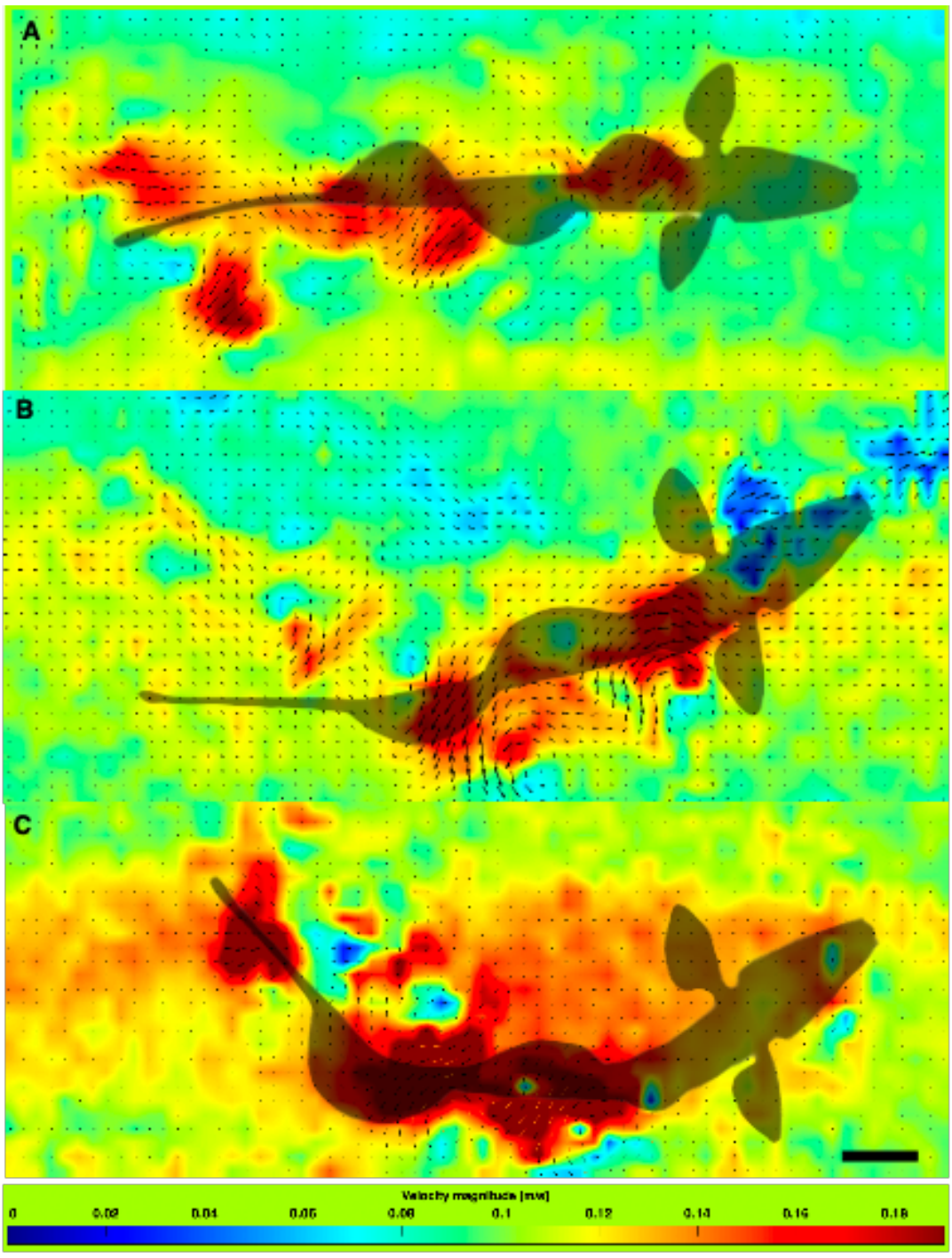

Fig. S1. Velocity profile of the ribbon fin during steady swimming and turning maneuvers. Velocity magnitude (m s^{-1}) during steady swimming (A), small turn (B), and large turn treatments (C). Fish silhouettes show the relative location of the fish with the ribbon fin intersecting the laser sheet. Scale bar represents 1 cm.

Table S1. Number of sequences analyzed per treatment by individual for kinematic analysis. Individual number corresponds to the Fish ID with 6 individuals total used in analysis. The number of useable sequences analyzed for each individual for each treatment is recorded along with the total sequences analyzed for each treatment.

Treatment	Individual number						Total sequences
	1	4	5	6	9	10	
Steady swimming	7	6	7	7	6	5	38
Small turn	7	7	7	9	7	6	43
Large turn	6	5	7	8	6	6	38

Table S2. Kinematic variables for the body, pectoral fins, and ribbon fin. Results of kinematic measurements for each maneuver performed by *Apteronotus albifrons* (N=6). Results are reported here as mean± s.d. (standard deviation) using the means of all individuals during steady swimming, small turns, and large turns. Superscript letters correspond to statistical significance among maneuvers determined by adjusted p-values from Bonferroni pairwise comparison tests following a One-Way Repeated Measures ANOVA ($\alpha = 0.05$).

Kinematic variable	Steady Swimming	Small maneuver	Large maneuver
Pitch angle (°)	6.16 ± 4.89^{a}	$-0.38 \pm 7.03^{a,b}$	-6.45 ± 4.19^{b}
Maximum yaw angle (°)	2.95 ± 1.50^{a}	16.5 ± 5.17^{b}	22.1 ± 7.08^{b}
Body bending coefficient	1.04 ± 0.03^{a}	1.10 ± 0.04^{b}	1.17 ± 0.05^{c}
Pectoral fin flapping frequency (Hz)	6.34 ± 5.23^{a}	6.38 ± 8.09^{a}	6.57 ± 4.63^{a}
Dorso-ventral pectoral angle (°)	43.95 ± 2.15^{a}	39.35 ± 3.30^{a}	42.37 ± 1.89^{a}
Asynchronous Index	0.48 ± 0.02^{a}	$0.38 \pm 0.04^{a,b}$	0.31 ± 0.04^{b}
Ribbon fin frequency (Hz)	$6.62 \pm 0.33^{a,b}$	6.64 ± 0.61^{a}	7.56 ± 0.64^{b}
Ribbon fin amplitude (°)	78.52 ± 15.54^{a}	68.85 ± 7.55^{a}	64.98 ± 16.03^{a}
Ribbon fin wavelength (cm)	0.43 ± 0.27^{a}	$0.86 \pm 0.37^{a,b}$	1.11 ± 0.25^{b}
Ribbon fin wave speed (cm s^{-1})	2.76 ± 1.80^{a}	5.66 ± 2.34^{b}	8.14 ± 0.61^{b}

Table S3. Results of Repeated Measures ANOVA. Results showing the effect of treatment on each kinematic variable across the three maneuvers performed by *Apteronotus albifrons* (N=6). Data used for this analysis consists of the averages for each variable per individual. Differences are considered significant when $p < 0.05$).

Kinematic variable	F statistic	p value
Pitch angle (°)	6.45	0.02
Maximum yaw angle (°)	40.24	< 0.0001
Body bending coefficient	43.22	< 0.0001
Pectoral fin flapping frequency (Hz)	0.36	0.71
Dorso-ventral pectoral fin angle (°)	0.64	0.55
Asynchronous Index	7.87	< 0.01
Ribbon fin frequency (Hz)	5.35	0.03
Ribbon fin amplitude (°)	2.44	0.14
Ribbon fin wavelength (cm)	7.84	< 0.01
Ribbon fin wave speed (cm/s)	12.41	<0.01

Table S4. Canonical Discriminant Analysis standardized coefficients. Data used in this analysis represent individual observations from six individuals during steady swimming, small turns, and large turns. Canonical Axes 1 and 2 explain the most variation in the data, and the resulting standardized coefficients for each variable are reported. Coefficients greater than or equal to |0.3| are bolded and are considered significant contributors to separation on the respective axis.

Kinematic variable	Canonical Axis 1	Canonical Axis 2
Pitch angle (°)	-0.28	**-0.36**
Maximum yaw angle (°)	0.20	0.51
Body bending coefficient	**0.70**	**-0.70**
Pectoral fin flapping frequency (Hz)	0.05	-0.13
Asynchronous Index	-0.14	0.05
Ribbon fin frequency (Hz)	**0.60**	**0.39**
Ribbon fin amplitude (°)	0.06	-0.16
Ribbon fin wavelength (cm)	**1.05**	**2.05**
Ribbon fin wave speed (cm/s)	**-0.74**	**-1.83**

Table S5. Average vortex size across treatments. The average vortex size (mm^2) sampled from *A. albifrons* (N=2) across steady swimming, small turn, and large turns. Data is presented as mean ± s.d. (standard deviation). Both clockwise and counterclockwise vortices were sampled from each fish during each treatment.

Treatment	Vortex size (mm^2)	Number of vortices sampled
Steady swimming	0.17 ± 0.036	14
Small turn	0.32 ± 0.011	22
Large turn	0.50 ± 0.016	14

Movie 1. Ventral view of all treatments. VideoS1_treatments.mp4 [(0:00-0:15 s) *A. albifrons* swimming behind a stationary feeder. (0:16-0:24 s) *A. albifrons* following the oscillating feeder during the small turn treatment. (0:25-0:32 s) *A. albifrons* following the oscillating feeder during the large turn treatment.

IndividualxTreatment_HawkinsJimenezSanford_2021.xlsx [Data set used for statistical analysis including the means of each fish (N=6) per each treatment.]

AllObservations_HawkinsJimenezSanford_2021.xlsx [Data set with compiled means from each digitization sequence for each treatment for each fish (N=6)].

RawDataSet_fishxtreatment_HawkinsJimenezSanford_2021.xlsx [Data set with all calibrated digitization coordinates in the x, y, and z planes for each analyzed sequence. Small turn files can be found in sheets 1-43, large turn files can be found in sheets 44-80, and steady swimming files can be found in sheets 81-118. Point 1 (tip of snout], Point 2 (end of head), Point 3 (body point in between pectoral fins), Point 4 (body point), Point 5 (body point), Point 6 (caudal peduncle), Point 7 (tip caudal fin), Point 8 (left pectoral fin tip), Point 9 (left pectoral fin base), Point 10 (right pectoral fin tip), Point 11 (right pectoral fin base), Point 12 (ribbon fin tip), Point 13 (ribbon fin base corresponding to Point 12), Point 14 (ribbon fin tip of a contiguous wave).]